Optics and Lasers in Engineering 51 (2013) 197–212

Contents lists available at SciVerse ScienceDirect

Optics and Lasers in Engineering

journal homepage: www.elsevier.com/locate/optlaseng

Accurate and robust estimation of camera parameters using RANSAC

Fuqiang Zhou *, Yi Cui, Yexin Wang, Liu Liu, He Gao

Key Laboratory of Precision Opto-mechatronics Technology, Ministry of Education, Beihang University, Beijing 100191, China

ARTICLE INFO

Article history:
Received 15 June 2012
Received in revised form
12 October 2012
Accepted 20 October 2012
Available online 11 November 2012

Keywords:
Camera calibration
Robust estimation
RANSAC
Machine vision

ABSTRACT

Camera calibration plays an important role in the field of machine vision applications. The popularly used calibration approach based on 2D planar target sometimes fails to give reliable and accurate results due to the inaccurate or incorrect localization of feature points. To solve this problem, an accurate and robust estimation method for camera parameters based on RANSAC algorithm is proposed to detect the unreliability and provide the corresponding solutions. Through this method, most of the outliers are removed and the calibration errors that are the main factors influencing measurement accuracy are reduced. Both simulative and real experiments have been carried out to evaluate the performance of the proposed method and the results show that the proposed method is robust under large noise condition and quite efficient to improve the calibration accuracy compared with the original state.

1. Introduction

Camera calibration is arguably one of the most classic and fundamental problems in computer vision (and photogrammetry), which has been studied extensively for decades [1]. According to Tsai's definition [2], camera calibration is the process of determining the internal camera geometric and optical characteristics (intrinsic parameters) and/or the 3D position and orientation of the camera frame relative to a certain world coordinate system (extrinsic parameters). Currently, various camera calibration algorithms have been reported [3] and existing methods have provided us with many choices to solve this problem in different settings. However, for general circumstances, the calibration methods frequently chosen for experimentation were developed by Tsai [2], Heikkila [4] and Zhang [5] since the source code for the three methods is publicly available, well developed and well tested [6]. Specifically, Tsai presented a radial alignment constraint (RAC) calibration method based on the two-step technique and this method requires accurate 3D coordinate measurement with respect to a fixed reference; Heikkila's method, also world-reference based, employs the more general direct linear transformation (DLT) technique by making use of the prior knowledge of intrinsic parameters; Unlike Tsai or Heikkila's methods that require a very precise 3-D reference object, Zhang's method is a flexible calibration technique by observing a planar target for at least twice, which might be the most convenient calibration method with enough accuracy developed so far [7].

No matter what method adopted, accurate calibration of camera is quite significant [8], since the calibration results determine the mapping relationship between 3D reference coordinate and 2D image coordinate. In many cases, especially for applications based on triangulation such as stereovision [9] or structure light vision [10], the overall performance of the machine vision system strongly depends on the accuracy of the camera calibration [11]. That is to say, the accuracy of the camera parameters will severely affect the implementation result of a subsequent vision task. For example, the reconstructed shape of an object may be deformed, the virtual object and the real object cannot be coincident, or the measurement will have low accuracy [12].

Normally, the factors that influence the calibration accuracy originate from various aspects, such as the extraction of feature points in the image plane, the geometric accuracy of the calibration target, the lens distortion model, the optimization algorithms used to converge on the camera parameters, and the operational conditions of the experiments. These aspects have been addressed, respectively, by designing an appropriate control markers or calibration target [13,14], by investigating the choice of calibration pattern [15], by improving the extraction precision of the feature points [16,17],by compensating for manufacturing errors of the calibration target [13], by calibrating lens distortion model separately [18–20], by adopting different optimization algorithms [5,21–23], by minimizing calibration errors in "distortion free" space or 3D space [24,25], and by setting the calibration process under optimal conditions [26]. However, to the best of our knowledge, there is little report about dealing with the unreliable feature points except for Ref. [12]. In Ref. [12], a filtering RANSAC method is proposed to

* Corresponding author. Tel./fax: +86 10 82339281.
E-mail address: zfq@buaa.edu.cn (F. Zhou).

0143-8166/$ - see front matter © 2012 Elsevier Ltd. All rights reserved.
http://dx.doi.org/10.1016/j.optlaseng.2012.10.012

remove the points with overlarge noise or mismatched. The author's objective is to improve the robustness of the commonly used DLT calibration method [4,27–29] that requires a very precise 3D target. However, up to now, the similar problem has not been solved in Zhang's calibration method [5] based on 2D planar target, whereas it is applied widely in plenty of vision measurement process. By using Zhang's method, a large quantity of feature points in several calibration images is required. Actually, it is well-known that it is difficult to accurately and reliably extract all wanted features in all images in the presence of noise, occlusion, image blur, and change of illumination or viewpoint [1]. Therefore, detecting and removing the unreliable image points (also called "outlier" in RANSAC) for camera parameter estimation and giving the corresponding solutions become an extremely important work. In this paper, we will cope with this problem in the following two steps: firstly, a simple threshold selection method is performed to choose the evident incorrect points by calculating re-projection error of each point and secondly, the RANSAC method is employed to remove the points with overlarge noise in each calibration image individually. After each step, all the camera parameters consisting of intrinsic, extrinsic and distorted parts are refined by Levenberg–Marquardt algorithm without the identified outliers. Finally, different evaluation functions are utilized to assess both the accuracy and robustness of the upgraded parameters. The advantages of our method include: (1) most of the outliers could be automatically recognized in all the calibration images; (2) the distribution and proportion of the outliers do not need to be prior known; (3) the camera parameters only need to be optimized after each removal operation; (4) the simple threshold selection method is capable of excluding some of the erroneous points easily before RANSAC.

The organization of the paper is as follows. Section 2 gives some preliminaries of RANSAC method. The detailed procedure of how to detect and remove the unreliable points during the calibration process is described in Section 3. Section 4 provides a few accuracy evaluation functions to assess calibration results. In Section 5, both computer simulative and real data are used to validate the proposed method. The paper ends with some concluding remarks in Section 6.

2. Preliminaries

The Random Sample Consensus (RANSAC) algorithm introduced by Fishler and Bolles [30] in 1981 is a simple and powerful technique that is widely applied to the task of estimating the parameters of a model in the field of computer vision, such as homograph estimation [31,32], fundamental matrix estimation [33–35], camera parameters estimation [12,36], motion estimation [37–39], image registration [40,41], shape alignment [42], geometric primitive recovery [43], projective reconstruction [44], ellipse extraction [45] and plane fitting [46]. RANSAC operates in a hypothesize-and-verify framework [47] which is opposite to that of conventional smoothing techniques: Rather than using as much of the data as possible to obtain an initial solution and then attempting to eliminate the invalid data points, RANSAC uses as small an initial data set as feasible and enlarges this set with consistent data when possible [30]. The standard RANSAC algorithm proceeds mainly as follows: Repeatedly, a minimal subset of the input data is randomly selected and model parameters fitting these subsets are computed. Then the model is evaluated on the entire dataset and its support (the number of data points consistent with the model) is determined. The hypothesize-and-verify loop is terminated when the probability of finding a better model becomes lower than a user-specified probability. The brief mathematical description of the RANSAC algorithm is described as follows:

Summary of RANSAC algorithm

Input: a data set of S_{all} which contains outliers; a model described by a series of parameters P

Output: the largest consensus set S_{con}; the model parameters P^* computed from S_{con}

(1) Randomly select a minimum subset $S^i_{\text{sub}} \subset S_{\text{all}}$ and initiate the model;

(2) According to a distance threshold t of the model, divide the data set S_{all} into S^i_{in} and S^i_{out} which satisfy $S^i_{\text{in}} \cup S^i_{\text{out}} = S_{\text{all}}$ and $S^i_{\text{in}} \cap S^i_{\text{out}} = \emptyset$;

(3) If the number of inliers $Num\left(S^i_{\text{in}}\right) > T$, then $S_{\text{con}} = S^i_{\text{in}}$, go to step(5);

(4) If the number of samples $i > N$, the largest consensus set S_{con} is selected, go to step (5); else $i = i+1$, go to step(1);

(5) The model parameters P^* is calculated from all the data in S_{con}.

In the above algorithm, the three thresholds t, T, and N are fully discussed in Ref. [29]. Particularly, the number of samples N is chosen sufficiently high to ensure with a probability, p, that at least one of the random samples of s points is free from outliers. Thus, the expression of N is given as:

$$N = \frac{\log(1-p)}{\log\left(1-(1-\varepsilon)^s\right)} \tag{1}$$

where, p is the requested probability of success, ε is the proportion of outliers, and s is the size of each sample, respectively. A summary of the number of RANSAC iterations needed as a function of the percentage of outliers ε is shown in Table 1. These values were obtained assuming a probability of success $p=99\%$ and the number of minimal data points $s=4$.

Apart from the standard RANSAC, there have been a number of recent efforts aimed at increasing the efficiency of the basic RANSAC algorithm, such as randomized RANSAC [48,49], RANSAC for (quasi-)degenerate data [50], and sufficient random sample coverage [51], etc. The modified framework mentioned above is suitable for use in real-time applications with a limited time budget or in special cases. However, in this paper, we have not yet considered the modification of the RANSAC algorithm since our primary goal is to introduce the RANSAC technique to depress the impact of the input data noise in Zhang's calibration method [5] and improve the accuracy of the camera parameters. Moreover, most camera calibration process is carried out off-line and the current computer's speed is high enough for most cases, thus we consider the computation cost is not a major factor to take into account.

3. Camera parameters estimation

In this section, we describe in detail how to detect and handle the inaccurate feature points by applying RANSAC to Zhang's calibration technique [5]. The whole process of the proposed approach is divided into two stages. At the first stage, we carry out a simple threshold selection method to wipe out some obviously

Table 1
The required number of samples with respect to outlier percentage.

Sample size	Percentage of outliers					
s	10%	20%	30%	40%	50%	60%
4	5	9	17	34	72	178

erroneous points, and then an adaptive RANSAC algorithm presented in [29] is used to cope with the other contaminated points with relative low level noise. Through the exhaustive removing for outliers, the contaminated feature points in each image are excluded before parameter optimization process starts. Then the original camera parameters can be updated to a precise state which will be demonstrated by our experiment. Further discussion of the accuracy evaluation standards is deferred until Section 4.

3.1. Camera model

The ideal pin-hole camera model is represented by a relationship between a 3D point $\boldsymbol{M}$ and its image projection $\boldsymbol{m}$:

$$\lambda\tilde{\boldsymbol{m}} = \boldsymbol{A}(\boldsymbol{R}|\boldsymbol{t})\tilde{\boldsymbol{M}}, \text{ with } \boldsymbol{A} = \begin{bmatrix} f_x & 0 & u_0 \\ 0 & f_y & v_0 \\ 0 & 0 & 1 \end{bmatrix} \tag{2}$$

where λ is an arbitrary scale factor, $\tilde{\boldsymbol{m}}$ and $\tilde{\boldsymbol{M}}$ are the homogeneous coordinates of image point and its corresponding space point, $(\boldsymbol{R},\boldsymbol{t})$, called the extrinsic parameters, is the rotation and translation which relates the world coordinate system to the camera coordinate system, and $\boldsymbol{A}$ is the camera intrinsic matrix, consisting of four parameters: f_x and f_y the effective focal length, (u_0,v_0) the coordinates of the principal point. Actually, real lenses do not satisfy the pinhole model and usually exhibit some degree of geometric distortion [52]. Considering the first two terms of radial distortion, we choose the following model to handle lens distortion effects:

$$\boldsymbol{m}_d = [1 + k_1 r^2 + k_2 r^4]\boldsymbol{m} \tag{3}$$

where, r is the distance from undistorted image point $\boldsymbol{m}$ to the principal point, k_1 and k_2 are the coefficients of the radial distortion, and $\boldsymbol{m}_d$ denotes the coordinates of distorted image point. Eqs. (1) and (2) completely describe the real perspective projection model of camera including lens distortion effects. The camera parameters including distortion coefficients can be calibrated with multiple views of the planar target by applying the calibration algorithm described in Ref. [5]. Note that all the views of the planar target are acquired by one camera in different

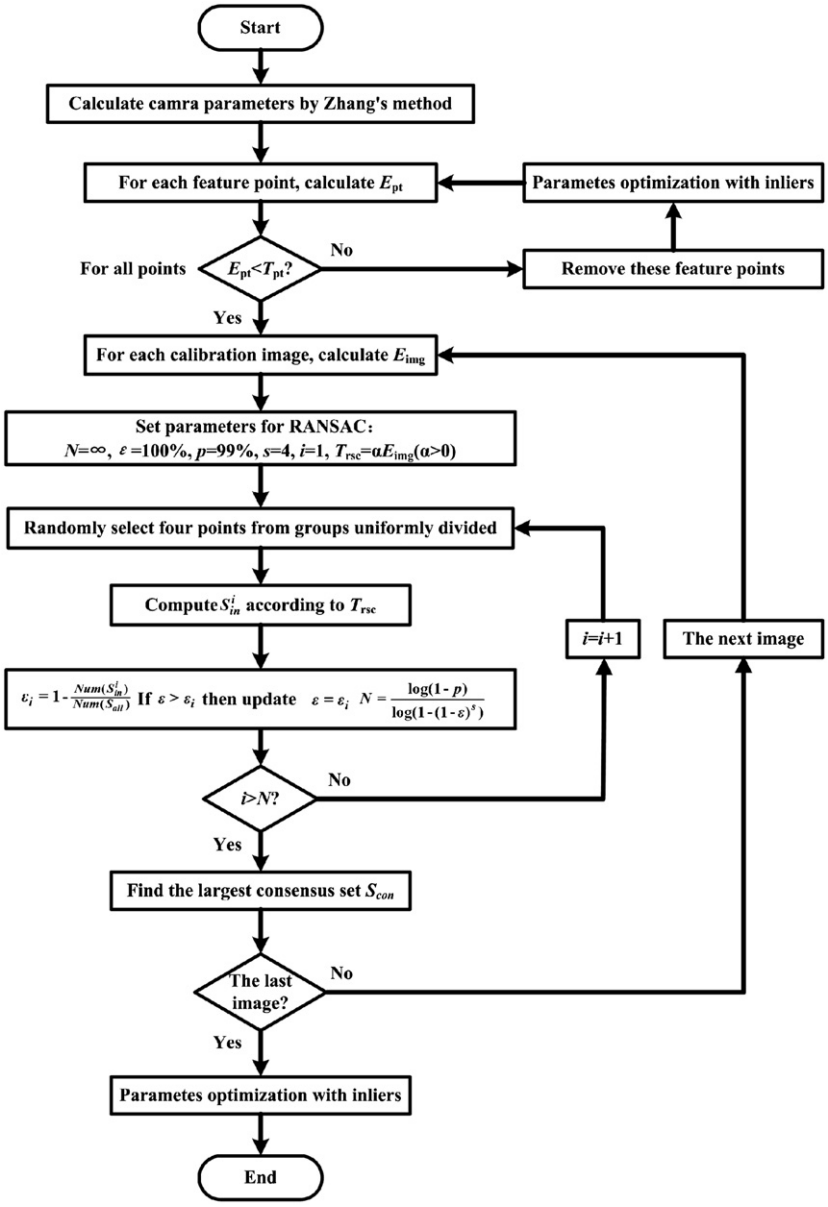

Fig. 1. Flow chart of the proposed method for accurate and robust estimation of camera parameters.

positions, thus each view has separate extrinsic parameters, but common intrinsic parameters and distortion coefficients.

3.2. Parameters estimation based on RANSAC

From the practical point of view, there often exist quite a few factors that may influence the localization precision of detected image points, such as uneven illumination environment, the contaminants on the surface of target or camera lens, the corner detectors' performance, etc. This means that the inaccurate or even erroneous information about the feature points in image plane would lead to inaccurate camera parameters if they are involved in the calibration process. Therefore, we need to exclude the feature points with overlarge noise (called outliers in RANSAC) before calibration. The crucial problem of how to detect and handle the outliers is what we will focus on. The detailed solution for this problem is described in the following.

Firstly, after normal camera calibration procedure completed, we can transform the known 3D feature point $\boldsymbol{M}$ in world coordinate system to image plane by applying the value of camera parameters. The re-projected image point calculated by us is expressed as $\boldsymbol{m}_p$. If the feature point on the image plane is exactly localized, the discrepancy between the detected point $\boldsymbol{m}_d$ and the re-projected point $\boldsymbol{m}_p$ is relatively not distinctive. However, it is not the case in practice. This is because, on the one hand, the detected point $\boldsymbol{m}_d$ has deviated from its real position in some degrees, and on the other hand, the acquired camera parameters could be inaccurate. Considering the fact that the difference between $\boldsymbol{m}_d$ and $\boldsymbol{m}_p$ could reflect the accuracy of both the image point and camera parameters, we decide to set a suitable distance threshold T_{pt} to select a part of outliers with extremely large deviation. That is to say, if the distance between $\boldsymbol{m}_d$ and $\boldsymbol{m}_p$, defined as E_{pt}, is greater than T_{pt}, the corresponding feature point is identified as outlier. After that, Levenberg–Marquardt algorithm is adopted to solve the nonlinear optimization problem for camera parameters which aims at minimizing the discrepancy between the two sets of image points without outliers. The objective function is presented in the following form:

$$\sum_{i=1}^{N}\sum_{j=1}^{L_i}\left\|\boldsymbol{m}_{d,i,j}-\boldsymbol{m}_{p,i,j}(f_x,f_y,u_0,v_0,k_1,k_2,\boldsymbol{R}_i,\boldsymbol{t}_i)\right\|^2 \tag{4}$$

where the subscript i denotes the sequence number of images and the subscript j denotes the sequence number of points in each image. It is worth noting that the determined outliers are excluded in the optimization process and the total number of image points L_i in the ith image is varied for each other. The first iteration requires an initial guess of camera parameters which can be obtained using the technique described in the previous section. This simple threshold selection step for seriously contaminated feature points is repeated until all the inliers are within the scope of distance threshold T_{pt}. In addition, we want to indicate that the choice of T_{pt} value depends on the practical situations, and in this paper we set $T_{\mathrm{pt}}=2$ pixel. A relatively high threshold is suggested since a very low threshold may cause instability in some cases and more sophisticated operation for outliers that contain relatively low noise can be disposed by RANSAC method.

Note that the simple threshold selection method is unable to find some outliers with relatively minor error, RANSAC method is employed to overcome this difficulty. In general, the RANSAC method provides a generative solution by randomly and repeatedly choosing a subset of data samples to generate a hypothesized model and testing the goodness of model fitting. When the sampled data are all inliers, the hypothesized model may meet the objectives, i.e. separating inliers from outliers and minimizing the total inlier errors [33]. In this article, we mainly investigate the problem of how to utilize the RANSAC method to enhance the performance of the calibrated camera parameters. The detailed procedure is described in the following passages.

Different from the simple threshold selection stage which takes all the input data as a whole and set a unified threshold T_{pt}, RANSAC applied for outliers' removal is carried out individually for every separate calibration image. In other words, the final inliers for calibration are the sum of the largest consensus set S_{con} computed by RANSAC in each view. In our cases, for each view, four point pairs are enough for the determination of camera position and orientation from known correspondences of 3D reference points and their images [53], that is, the number of minimal data for random sampling is four. However, degenerate samples should be disregarded since it is possible that three of the four selected points are collinear. Besides, the sample should consist of points with a good spatial distribution over the image to ensure the mapping accuracy. Hence, distributed spatial sampling is implemented by tiling the image into several areas. In this paper, we divide the feature points into four almost uniform distributed groups according to their relative position in the image. For each sampling, four points is randomly provided by four different groups, respectively. Subsequently, the linear 4-points algorithm is adopted to calculate the rotation matrix and translation vector between the world coordinate system and camera coordinate system, that is, the newly estimated extrinsic parameters. Since the intrinsic parameters and distortion coefficients are determined by multiple views of calibration images, we can fix them as common parameters for each view. Thus, the newly obtained extrinsic parameters and the fixed common

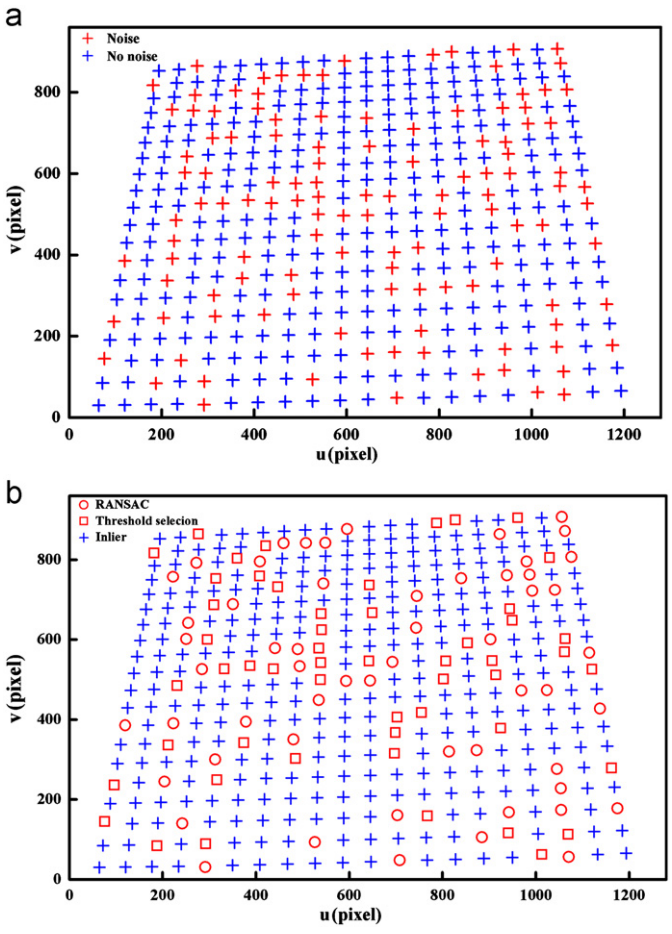

Fig. 2. A set of image points used for calibration: (a) simulated image points; (b) detected outliers obtained by the proposed method.

parameters constitute an instantiation of camera model for each sampling, and the new re-projected image point $\boldsymbol{m}_p$ in the same view is easily obtained from these parameters. In order to decide whether an unknown feature point belongs to inliers or not, the pixel distance between $\boldsymbol{m}_p$ and $\boldsymbol{m}_d$, denoted as E_{rsc}, is compared with the threshold T_{rsc}. The consensus set for each image is made of feature points that satisfy the inequality $E_{\mathrm{rsc}} < T_{\mathrm{rsc}}$. Note that it is often the case that ε, the fraction of data consisting of outliers, is unknown. To address this issue, we can determine the number of samples N adaptively and the repeated random sampling will terminate as soon as N samples have been performed. After that, the largest consensus set S_{con} has been established. The ultimate

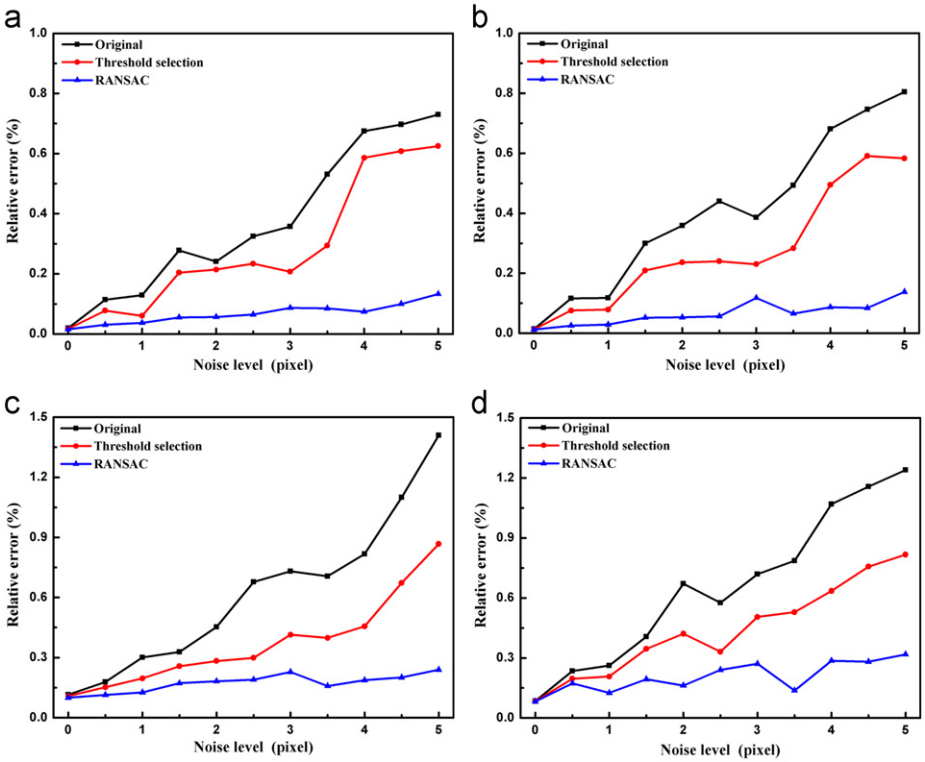

Fig. 3. Effects of pixel coordinate noise on intrinsic parameters: (a) f_x; (b) f_y; (c) u_0; (d) v_0.

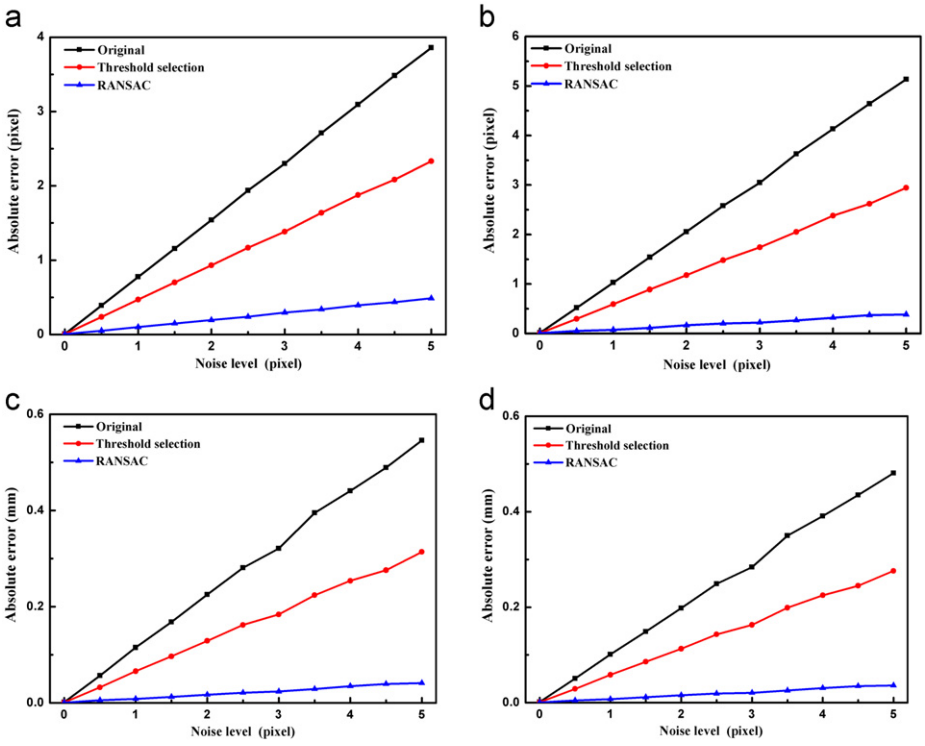

Fig. 4. Effects of pixel coordinate noise on calibration accuracy for training data: (a) E_{rms}; (b) E_{nce}; (c) E_{pt}; (d) E_{ray}.

inliers of feature points are composed of the largest consensus sets obtained from each image. Finally, according to Eq.(4), all the model parameters are upgraded again taking advantage of the computed inliers. Because of the delicate outlier removal, the undesirable effect that the outliers imposed on the calibration results is thoroughly eliminated.

Furthermore, we will discuss several critical issues involved in the process of robust estimation. (a) The necessity of the simple threshold selection before RANSAC implemented. Since the simple threshold selection is capable of removing a certain part of outliers effectively, the fraction of outlier ε is reduced to some extent when the RANSAC method is applied. So the number of

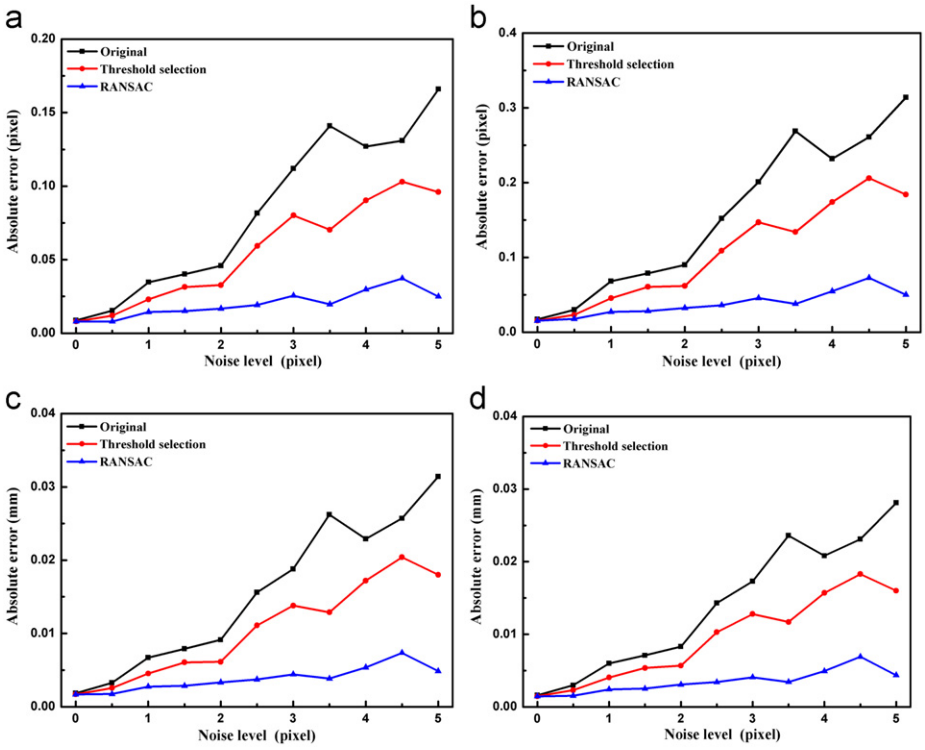

Fig. 5. Effects of pixel coordinate noise on calibration accuracy for testing data: (a) E_{rms}; (b) E_{nce}; (c) E_{pt}; (d) E_{ray}.

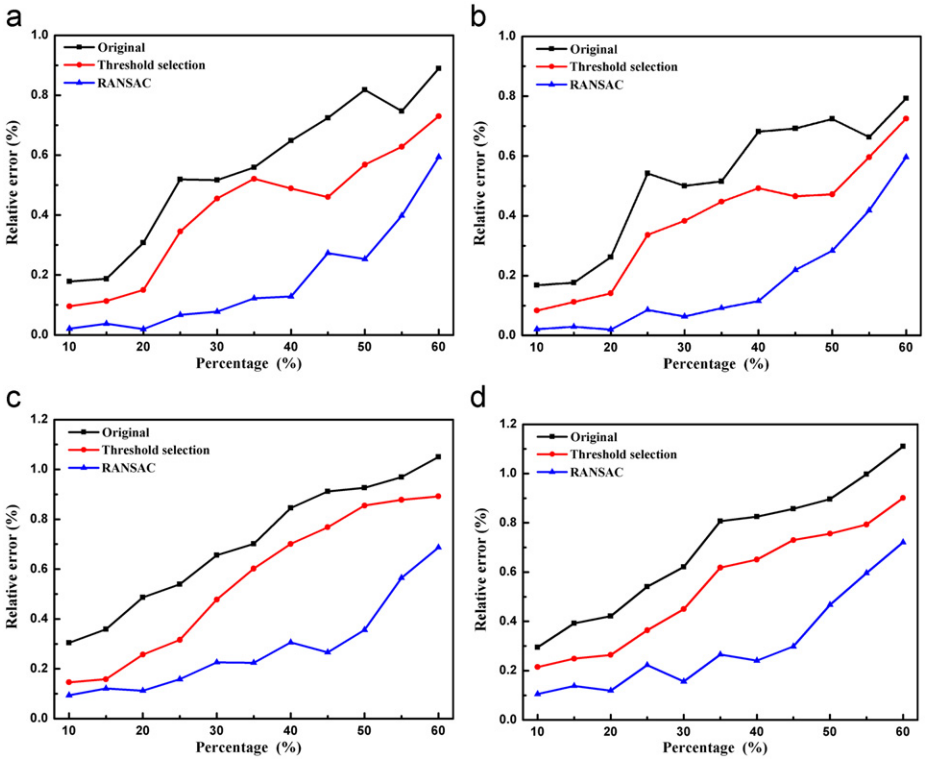

Fig. 6. Effects of outlier percentage on intrinsic parameters: (a) f_x; (b) f_y; (c) u_0; (d) v_0.

random samples N is also reduced according to the quantitative relationship described in Eq. (1), which is beneficial to the decrease of computation cost. (b) The choice of threshold T_{rsc}. It has been observed that the overall error level for one calibration image is different compared with others. Thus we set the value of threshold T_{rsc} according to the root mean square re-projection error E_{img} for the corresponding image. In this article, we choose T_{rsc} as $1.2E_{img}$. Of course, the scale factor between T_{rsc} and E_{img} could be adjusted more or less with the change of actual condition, arising from the possibly unknown or unmodelled error distribution. (c) The noise condition of the selected four points. For each sampling, four points are randomly selected from groups uniformly divided according to their relative position in the image. However, since the randomness of each sampling, whether

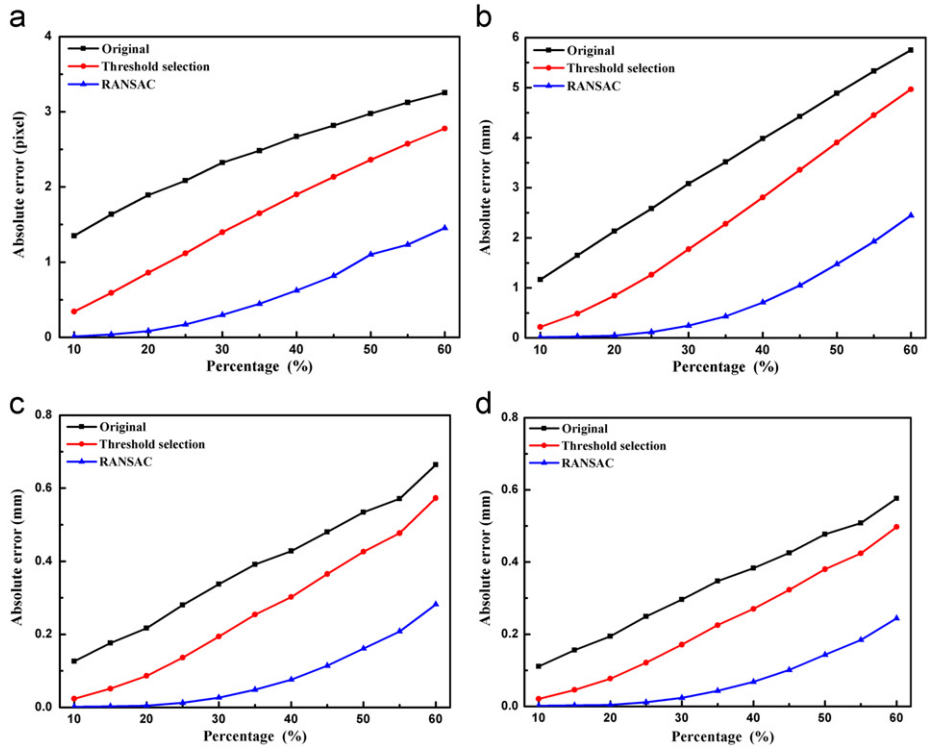

Fig. 7. Effects of outlier percentage noise on calibration accuracy for training data: (a) E_{rms}; (b) E_{nce}; (c) E_{pt}; (d) E_{ray}.

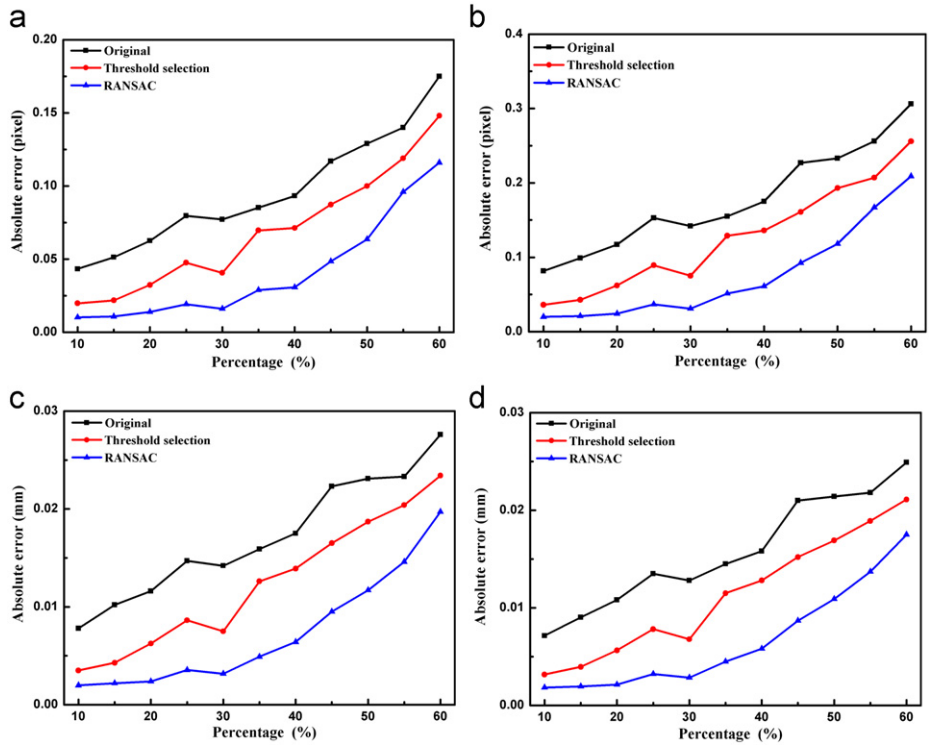

Fig. 8. Effects of outlier percentage noise on calibration accuracy for testing data: (a) E_{rms}; (b) E_{nce}; (c) E_{pt}; (d) E_{ray}.

all the points contain large noise or not is unknown for us. Therefore, the number of samples N is chosen sufficiently high to ensure with a probability, p (we choose $p=99\%$ in this article), that at least one of the random samples of four points is free from outliers. We can determine the number of samples N adaptively and the repeated random sampling will terminate as soon as N samples have been performed. The four feature points which have identified the largest consensus set is sure without large noise, with probability of success $p=99\%$. (d) The terminal condition for RANSAC. As described previously, the idea of "probing" the data via the consensus sets can be applied repeatedly in order to adaptively determine the number of samples, N. At first, the algorithm is initialized using a worst case estimate of $\varepsilon=100\%$, $N=\infty$, and this estimate can then be updated as larger consistent sets are found. The updated estimate of ε from the larger consistent sets determines a reduced N from Eq. (1). This update is repeated at each sample, and whenever a consensus set with ε lower than the current estimate is found, then N is again reduced. The RANSAC is terminated until the number of samples that have already been performed is greater than N. (e) The choice of the largest census set S_{con}. When the terminal condition is satisfied, the largest census set S_{con} is chosen as the one with the largest number of inliers. If there are two or more candidates with equal number of inliers, we can choose S_{con} as the census set that has the lowest re-projection error of inliers. (f) The handling for refining the camera parameters. Here, instead of conducting the calibration algorithm with inliers from the beginning, we adopt Levenberg–Marquardt non-linear optimization algorithm to upgrade parameters iteratively. This is because the approximate solution obtained by Zhang's method [5] is usually a good initial guess for the mentioned re-optimization approach even though the initial solution takes the outliers into account. (g) The distinction between the presented method and the robust homograph estimation. Seemingly, this process is somewhat similar to the robust homograph estimation. However, we should indicate that the homograph estimation takes no consideration of both the intrinsic parameters and distortion coefficients, and it merely deals with the 2D–2D point correspondence.

3.3. Summary

To sum up, the proposed estimation method for camera parameters based on RANSAC is illustrated as follows:

(1) Calculate the initial camera parameters by Zhang's method;
(2) Compute the re-projection error E_{pt} for each feature point and compare it with distance threshold T_{pt};
(3) Select the inliers when its E_{pt} is less than T_{pt}. Optimize the parameters with inliers iteratively according to Eq. (4). Step(2)–(3) is repeated until all the points satisfy $E_{\text{pt}} < T_{\text{pt}}$;
(4) Calculate the root mean square re-projection error E_{img} for a calibration image. Set parameters for RANSAC method: $T_{\text{rsc}}=\alpha E_{\text{img}}(\alpha>0)$, $N=\infty$, $\varepsilon=100\%$, $p=99\%$, $s=4$, $i=1$;
(5) Divide the feature points into four groups and randomly select a point from each group;
(6) Compute the model parameters from the selected four points. Identify a set of inliers consistent with these evaluated parameters according to T_{rsc};
(7) Update the upper limit of sample count N if a larger consistent set S_{in}^{i} is found;
(8) If the number of samples $i>N$, the largest consensus set S_{con} is selected, go to step(9); else $i=i+1$, go to step(5);
(9) If all the views for calibration have been handled, the largest consensus sets obtained from each image constitute the final inliers, go to step(10);else deal with the next image, go to step(4);
(10) Optimize the camera parameters with all the inliers.

The flow chart of the proposed method in this section can also be summarized as Fig. 1.

4. Accuracy evaluation

It is necessary to take appropriate measures to evaluate accuracy in terms of camera parameters, so we can immediately know whether the corresponding calibration is well done. To validate the effectiveness of our estimation method with regard to accuracy improvement, the available assessment criterions are employed. In the following text, some of the most frequently used methods of accuracy evaluation are described.

(1) The root mean square re-projection error [6] E_{rms}. It is computed by the discrepancy between estimated image point $(\hat{x}_{u,i},\hat{y}_{u,i})$, projected from world coordinate system by camera model with lens distortion, and the observed image point $(x_{u,i},y_{u,i})$ obtained from captured images directly:

$$E_{rms}=\frac{1}{n}\sum_{i=1}^{n}\sqrt{(x_{u,i}-\hat{x}_{u,i})^2+(y_{u,i}-\hat{y}_{u,i})^2} \tag{5}$$

where, n is the total number of feature points.
(2) The normalized calibration error [8] E_{nce}. Since E_{rms} are intuitive but sensitive to digital image resolution, camera

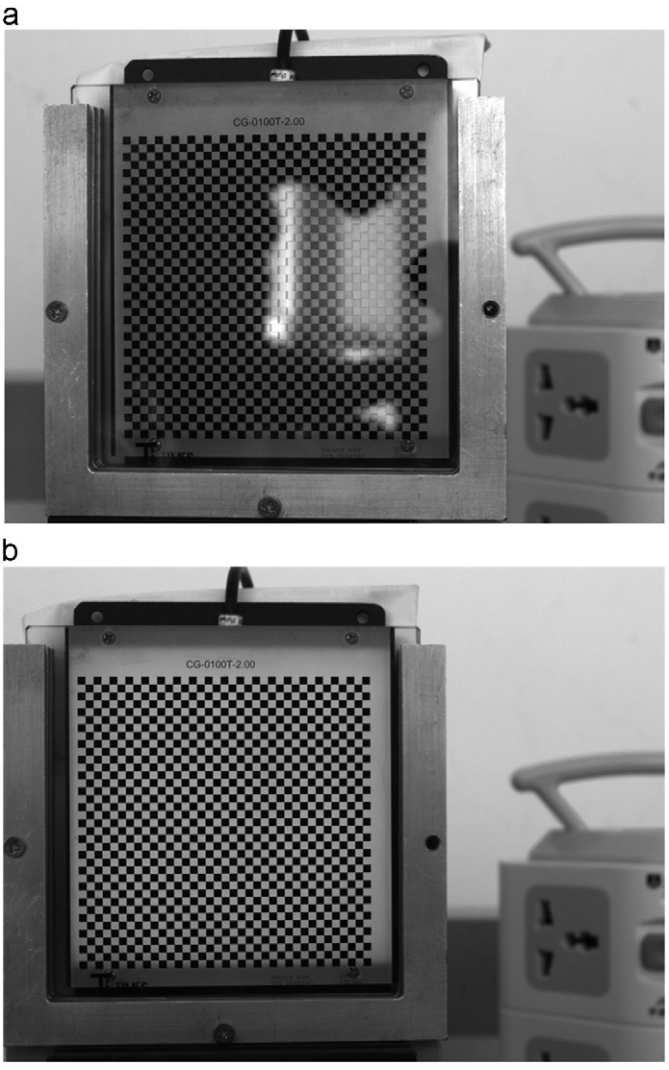

Fig. 9. Images captured in real experiment (a) training data; (b) testing data.

field-of-view, and object-to-camera distance [6], the normalized calibration errors proposed by Weng [8] overcomes this sensitivity by normalizing the discrepancy between estimated and observed 3D points with respect to the area each back-projected pixel covers at a given distance from the camera. The E_{nce} is defined as follows:

$$E_{\mathrm{nce}} = \frac{1}{n}\sum_{i=1}^{n}\sqrt{\frac{(x_{c,i}-\hat{x}_{c,i})^2+(y_{c,i}-\hat{y}_{c,i})^2}{z_{c,i}^2\left(f_x^{-2}+f_y^{-2}\right)/12}} \tag{6}$$

where, $(x_{c,i},y_{c,i},z_{c,i})$ represents the observed 3D camera coordinate of the ith point transformed from the world coordinate system and $(\hat{x}_{c,i},\hat{y}_{c,i},z_{c,i})$ represents the estimated 3D camera coordinate computed by back-projection from 2D corrected image point to depth $z_{c,i}$.The value of f_x and f_y can be calculated using the intrinsic camera parameters.

(3) Radius of ambiguity in the calibrating plane [54] E_{pt}. First, the position of the unknown target plane in camera coordinate system can be calculated by applying calibrated parameters. Second, the calibrated model is used to project the optical ray

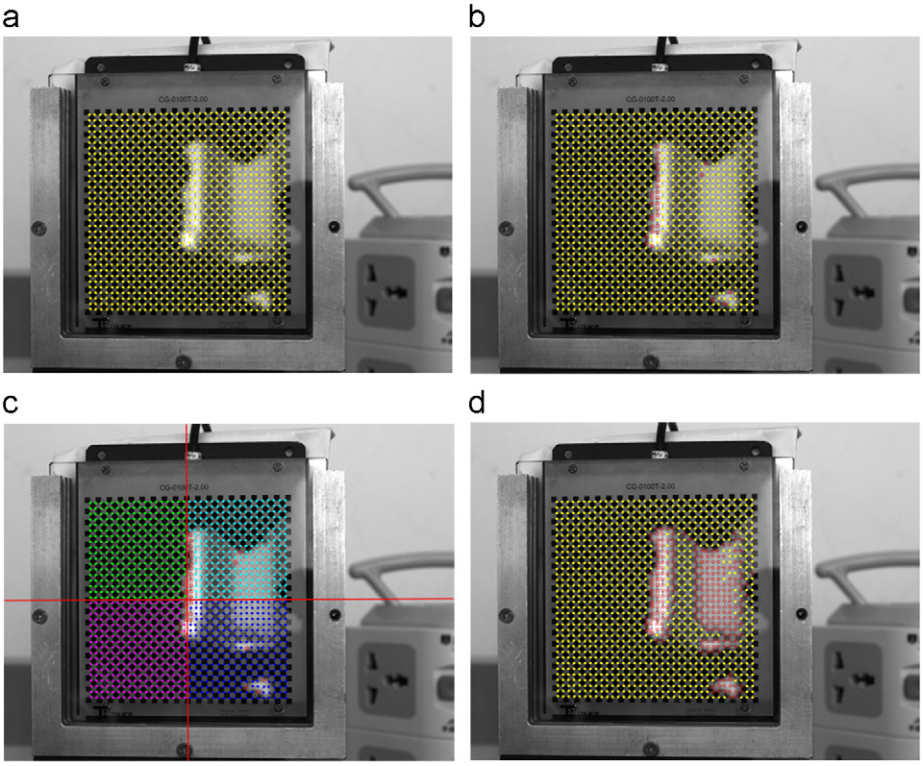

Fig. 10. The main procedure of outlier detection: (a) the original image with feature points; (b) the result after simple threshold selection; (c) the division of the residual points; (d) the final state after RANSAC method implemented. The red rectangle and circle represent the detected outliers by threshold selection and RANSAC, respectively.

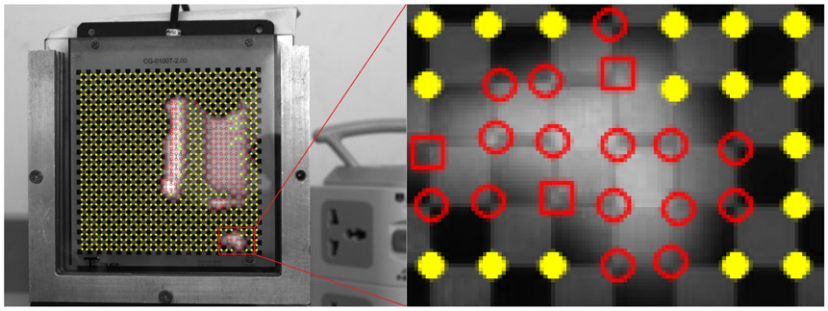

Fig. 11. The enlarged part of the outlier detection result.

Table 2
Comparative results of camera parameters and calibration accuracy.

State	f_x (pixel)	f_y (pixel)	u_0 (pixel)	v_0 (pixel)	k_1 (mm^{-2})	k_2 (mm^{-4})	E_{rms} (pixel)	E_{nce} (pixel)	E_{pt} (mm)	E_{ray} (mm)
Original	2672.92	2674.03	555.04	505.70	−0.0491	−0.869	0.752	1.197	0.102	0.100
Threshold	2687.32	2688.34	558.87	498.40	−0.0485	−0.996	0.547	0.963	0.0725	0.0722
RANSAC	2735.10	2735.77	591.01	488.21	−0.0962	−0.0764	0.240	0.368	0.0290	0.0286

back from the projection center and corrected image point. The transverse of the optical ray with the test target plane determines the intersection point. The distance from the 3D observed test point $\boldsymbol{M}_{c,i}$ to this intersection point $\hat{\boldsymbol{M}}_{c,i}$ defines a radius of ambiguity around the 3D feature point:

$$E_{\mathrm{pt}} = \frac{1}{n}\sum_{i=1}^{n}\sqrt{\|\boldsymbol{M}_{c,i}-\hat{\boldsymbol{M}}_{c,i}\|^2} \tag{7}$$

(4) Distance with respect to the optical ray [54] E_{ray}. The error criterion can be defined as the distance between the 3D observed test point $\boldsymbol{M}_{c,i}$ and optical ray $\hat{\boldsymbol{L}}_{c,i}$, which is back-projected from the corresponding corrected image point on the camera image plane. With this given, the E_{ray} is represented as:

$$E_{\mathrm{ray}} = \frac{1}{n}\sum_{i=1}^{n}\sqrt{\|\boldsymbol{M}_{c,i}-\hat{\boldsymbol{L}}_{c,i}\|^2} \tag{8}$$

5. Experimental results

In this section, the proposed estimation method for camera parameters has been tested on both computer simulated data and real data. A comparison with three different states, namely, "original state", "threshold selection" and "RANSAC", is carried out. Results are evaluated by comparing the computed camera parameter values with the simulated or physical ones and evaluating the calibration accuracy with both training data and testing data.

5.1. Computer simulation

Unlike Ref. [4] the simulative image is not synthesized in this experiment, rather only the point correspondence is simulated. The simulated camera's image size is 1280×960 pixels with the principal point at $(u_0, v_0)=(630,490)$ pixel. The skew factor is set to zero. The effective focal length along the x and y direction in pixels is $f_x=2000$ pixel and $f_y=2000$ pixel, respectively. A second-order radial distortion is simulated with the coefficients $k_1=-0.1\ \mathrm{mm}^{-2}$, $k_2=-0.08\ \mathrm{mm}^{-4}$. The training and testing model plane is a checkerboard target with 400 corners (20×20) uniformly distributed and the minimum point interval is 5 mm. The images are taken from 15 different orientations in front of the virtual camera. All the images are captured randomly in the range of the following position parameters: object-to-camera distance is 200∼400 mm and the angle between the target plane and the image plane is 0∼60°. Ten images are used to compute the parameters and five to test the results. Gaussian noise of mean

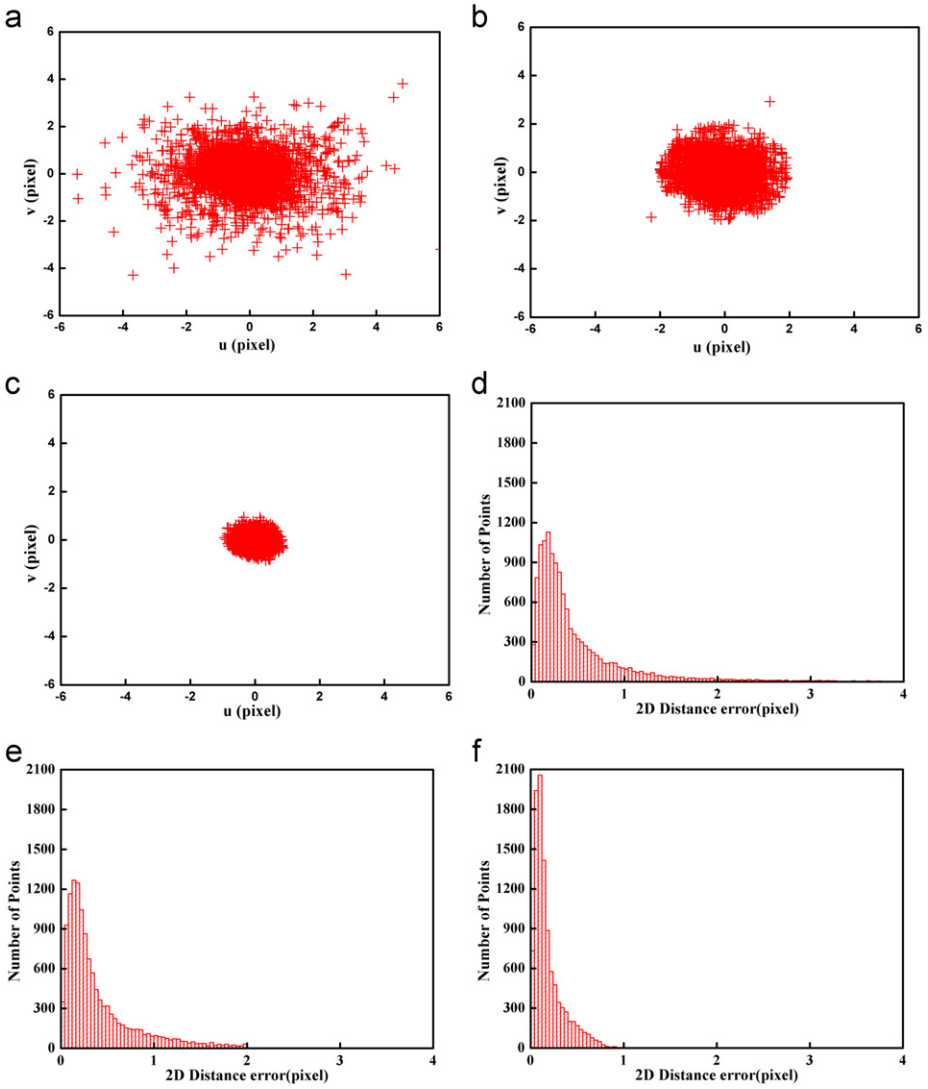

Fig. 12. 2D calibration error distribution and distance error statistics for training data at different states: original, threshold selection and RANSAC. (a)–(c): the re-projection error distribution for all the points (exclude outliers in (b) and (c)); (d)–(f): the 2D distance error statistics for all the points (exclude outliers in (e) and (f)).

0 and standard deviations ranged from 0 pixel to 5 pixel is added to the point's coordinates of the images. It is added to training data but no noise is added to test data. Note that only parts of points in training data are randomly chosen and added noise. For each noise level, we perform 25 independent trials, and the average results are shown in Figs. 3–8.

One of the training data used for calibration is shown in Fig. 2(a). The percentage of the outlier is set as 30% and the randomly selected image points are added a 3 pixel gauss noise. With the proposed method, most of the outliers are successfully detected by "threshold selection" and "RANSAC", respectively. It is clearly observed in Fig. 2(b) that the false positive rate for the outliers is zero. Namely, the points with no noise are not mistaken for outliers. However, several generated outliers are escaped from the detected results. This is because the deviations of these points from the real positions are too slight to be detected. It may occur that a noised point has not any deviation due to the property of the added gauss noise. In that case, the generated outlier is actually an inlier. For this reason, the non-zero false negative rate in our simulation is permissible.

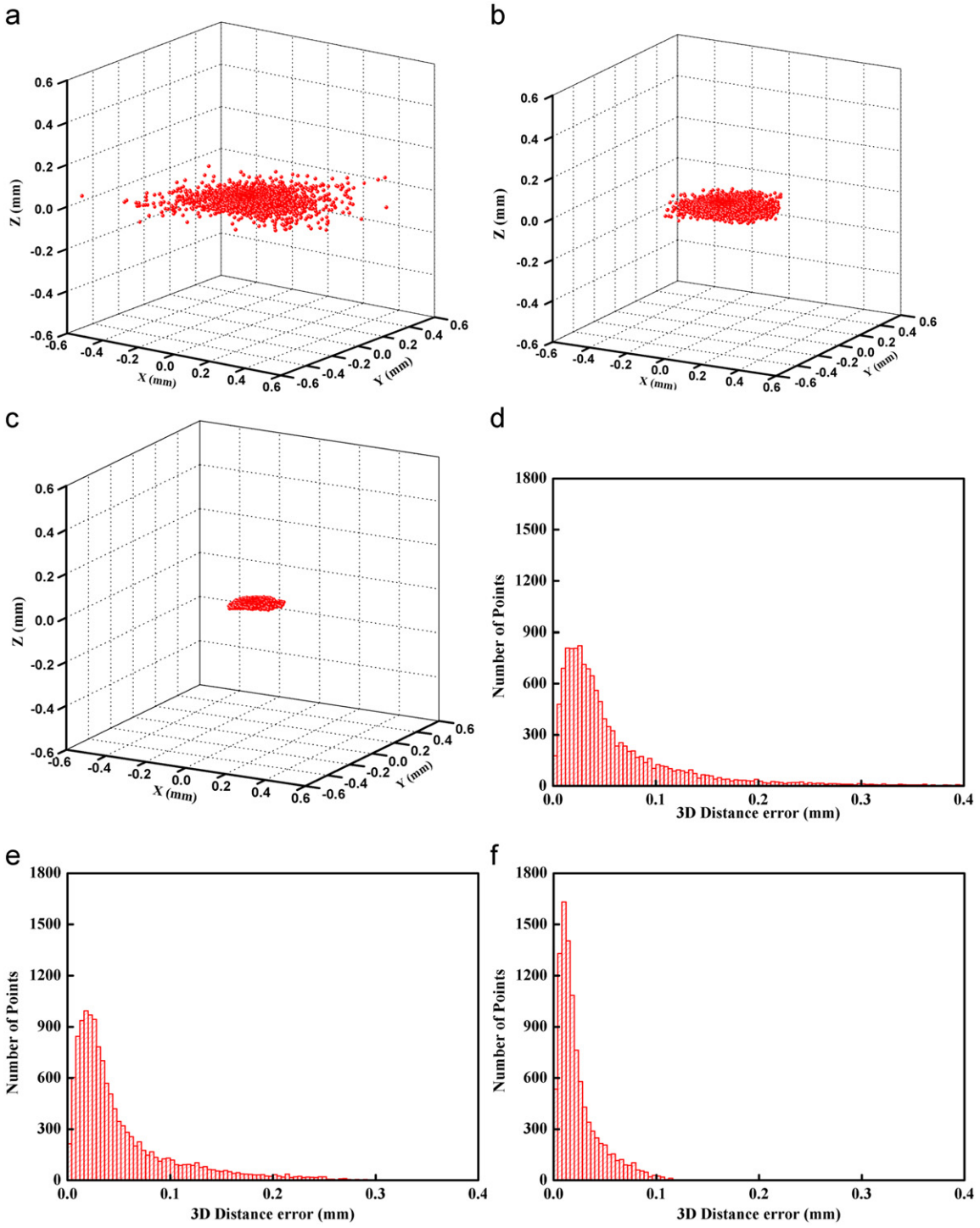

Fig. 13. 3D calibration error distribution and distance error statistics for training data at different states: original, threshold selection and RANSAC. (a)–(c): the 3D error distribution for all the points (exclude outliers in (b) and (c)); (d)–(f): the 3D distance error statistics for all the points (exclude outliers in (e) and (f)). The computation of 3D calibration error can be referred to Eq. (7).

Intrinsic parameters with respect to noise level: Fig. 3 shows the influence of noise on camera intrinsic parameters for three different states. The percentage of the outlier is set as a constant level of 30%. The estimated camera parameters are compared with the ground truth and we measure their relative errors with respect to the focal length f_x. This is because Triggs [55] has pointed out that the absolute errors in (u_0,v_0) is not geometrically meaningful, while computing the relative error is equivalent to measuring the angle between the true optical axis and the estimated one. As we can see, the relative error is dramatically reduced after threshold selection and RANSAC are utilized to deal with the original training data. With the noise level increasing, the error achieved by the proposed RANSAC method keeps in a very low level which demonstrates the robustness to the overlarge noise. Similar property can also be discovered in Figs. 4 and 5.

Calibration accuracy with respect to noise level: Figs. 4 and 5 illustrate the effect of noise level on calibration accuracy for training data and testing data, respectively. Fig. 4 reveals a strong linear relationship between calibration error, namely, E_{rms}, E_{nce}, E_{pt}, or E_{ray}, and noise level. As described in Section 4, E_{rms} and E_{nce} are established based on 2D image coordinates system, while E_{pt} and E_{ray} are constructed in 3D measurement coordinate system. Hence, tracing the variation of the above four evaluation functions could reflect the performance of calibration results in a more comprehensive way. It can be seen from Fig. 4 that the proposed estimation method reduces the calibration errors effectively even when the noise level is high enough. Since training data used for evaluation is also involved in calibration process, the testing data with unknown position is utilized to evaluate camera parameters obtained in different states. In this case, the extrinsic parameters for these testing data are calculated from the

Table 3
Comparative results of calibration accuracy for testing data.

State		Image 1	Image 2	Image 3	Image 4	Image 5	Average	Standard error
Original	E_{rms} (pixel)	0.110	0.140	0.135	0.163	0.141	0.138	0.00846
	E_{nce} (pixel)	0.232	0.303	0.284	0.356	0.306	0.296	0.0200
	E_{pt} (mm)	0.0144	0.0186	0.0179	0.0200	0.0170	0.0176	0.000934
	E_{ray} (mm)	0.0143	0.0182	0.0176	0.0195	0.0168	0.0173	0.000866
Threshold selection	E_{rms} (pixel)	0.104	0.124	0.123	0.147	0.132	0.126	0.00698
	E_{nce} (pixel)	0.220	0.266	0.262	0.324	0.288	0.272	0.0170
	E_{pt} (mm)	0.0136	0.0164	0.0165	0.0182	0.0159	0.0161	0.000740
	E_{ray} (mm)	0.0135	0.0161	0.0163	0.0177	0.0157	0.0159	0.000679
RANSAC	E_{rms} (pixel)	0.0763	0.0839	0.0822	0.115	0.0965	0.0908	0.00689
	E_{nce} (pixel)	0.163	0.180	0.176	0.251	0.217	0.197	0.0161
	E_{pt} (mm)	0.0100	0.0111	0.0110	0.0141	0.0116	0.0116	0.000686
	E_{ray} (mm)	0.00996	0.0109	0.0107	0.0138	0.0115	0.0114	0.000655

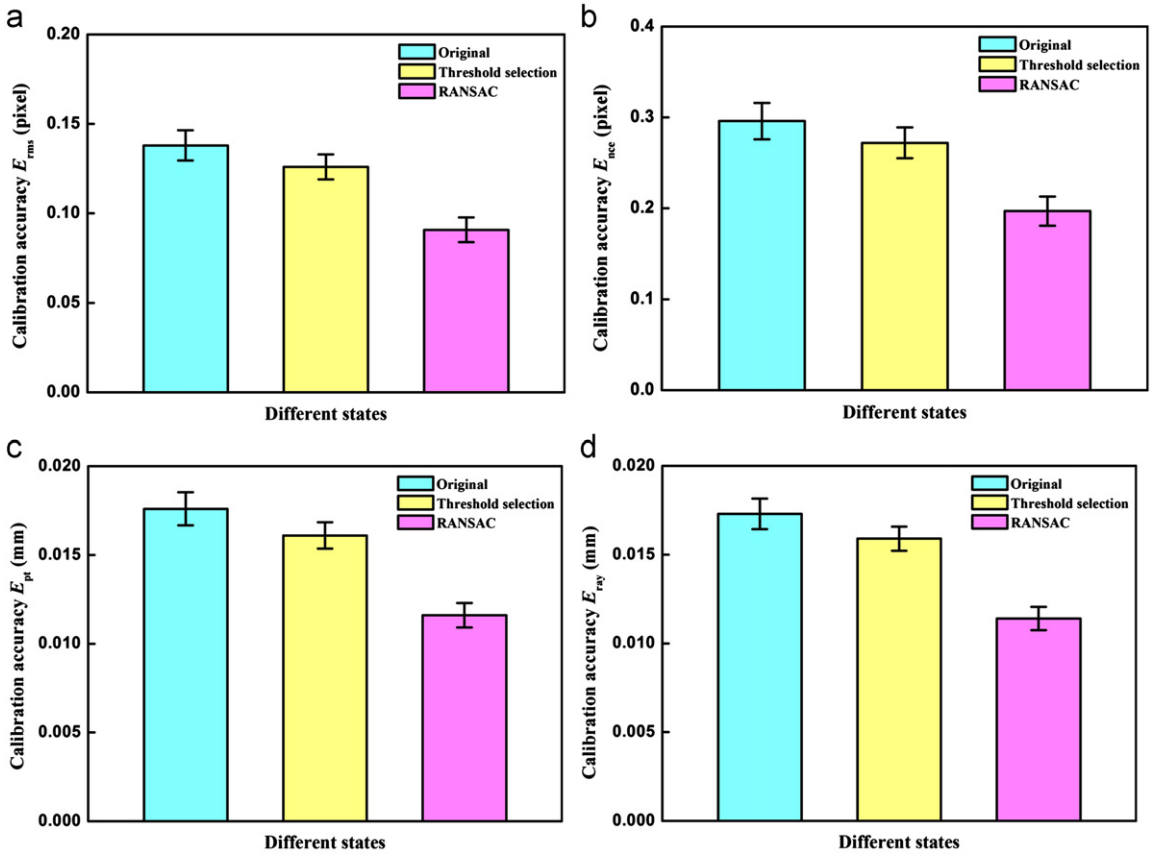

Fig.14. Comparative results of average calibration accuracy for testing data: (a) E_{rms}; (b) E_{nce}; (c) E_{pt}; (d) E_{ray}.

calibrated intrinsic ones and distortion coefficients, which is consistent with vision measurement process. From Fig. 5 we can observe that the variation tendency of calibration accuracy for testing data is similar to training data and the results obtained by our proposed method keeps a well stability with respect to noise level.

Intrinsic parameters with respect to outlier percentage: Fig. 6 shows the effect of outlier percentage on camera intrinsic parameters for three different states. The noise of the outlier is set as a constant level of 3 pixel and the outlier percentage is varied from 10% to 60%. It is noticeable that the relative error of intrinsic parameters is greatly reduced after outlier removal, especially when the outlier percentage is below 50%. However, we can easily find the fact that the relative error in the final state is increased rapidly when the outlier percentage is raised to 50% or above. This phenomenon can be explained as follows: when the outlier percentage is large enough, the E_{img} is raised to a relative high level correspondingly. However, in this paper, the distance threshold T_{rsc} is chosen as αE_{img} ($\alpha=1.2$) empirically, and the T_{rsc} is not high enough to exclude all the outliers in this case. If we change the value of α to a smaller value, this situation is improved obviously since RANSAC algorithm is able to cope with a large

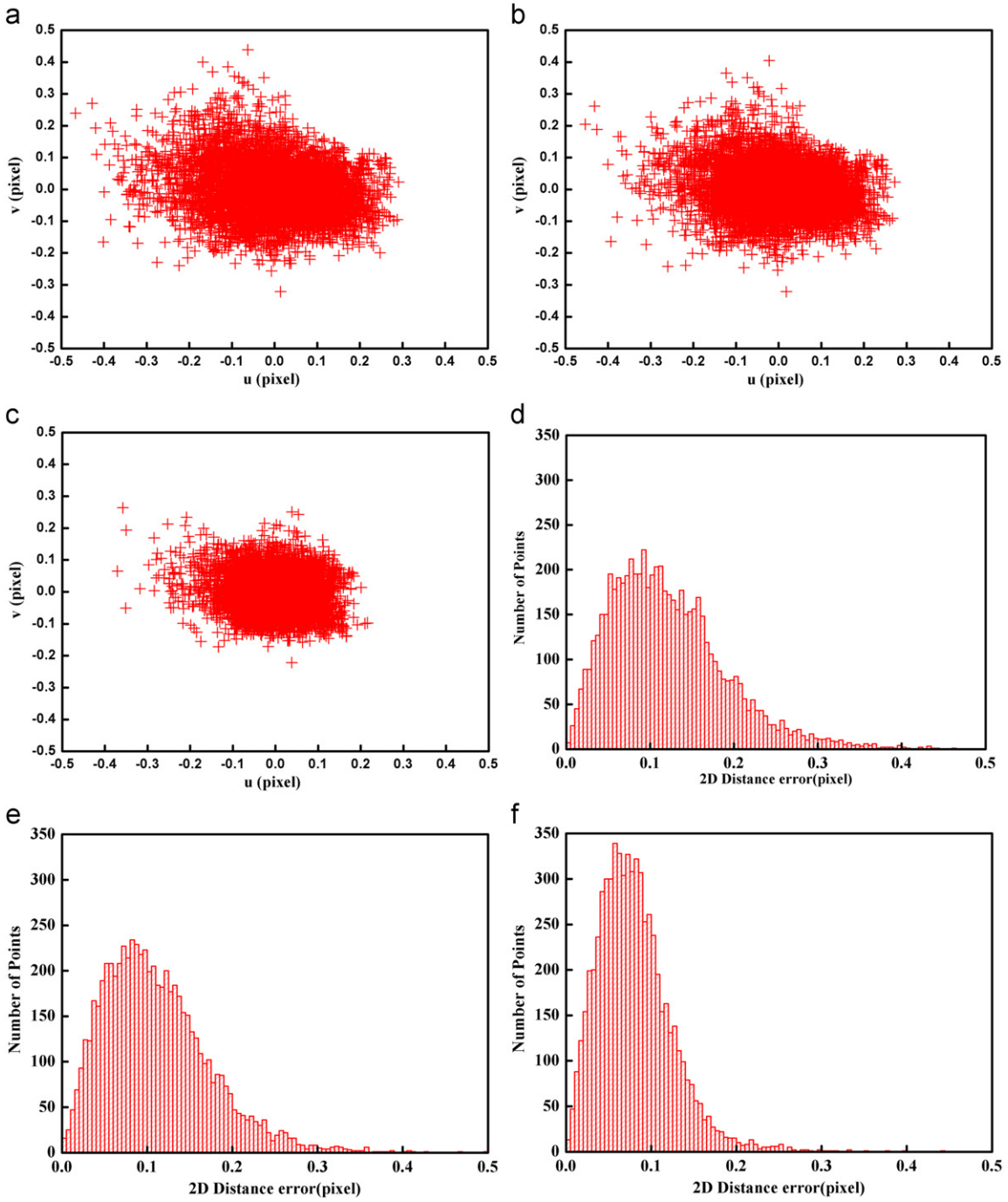

Fig. 15. 2D calibration error distribution and statistics for testing data at different states: original, threshold selection and RANSAC. (a)–(c): the re-projection error distribution for all the points; (d)–(f): the 2D distance error statistics for all the points.

proportion of outliers [29]. From a practical point of view, the cases that outlier percentage is more than 50% rarely happen, and therefore, taking consideration of efficiency, $\alpha=1.2$ is sufficient to deal with most situations.

Calibration accuracy with respect to noise level: Figs. 7 and 8 display the effect of outlier percentage on calibration accuracy for training data and testing data, respectively. Note that firstly the camera parameters is refined by simple threshold selection, and then upgraded by RANSAC again to a more accurate level. The calibration accuracy is improved step by step regarding to both training data and testing data. Like Fig. 6, the improvement for calibration accuracy is lessened when the outlier percentage is raised to 50% or above, which has been discussed previously.

5.2. Real data

For the experiment with real data, a camera consists of a CCD (Point grey FL2-20S4M/C) and lens (Computar) with 12 mm focal length is used, and the image resolution of the given camera is 1280×960 pixels. The calibration target is a planar chessboard pattern with 36×36 corner points evenly distributed. The size of the pattern is 74×74 mm^2 and the distance between the adjacent points is 2 mm in the horizontal and the vertical directions. The target is made of glass with manufacture accuracy of 0.001 mm. The images are taken from 15 different orientations. 10 of them are taken as training data and the other 5 are testing data. The training data and testing data are acquired under natural and

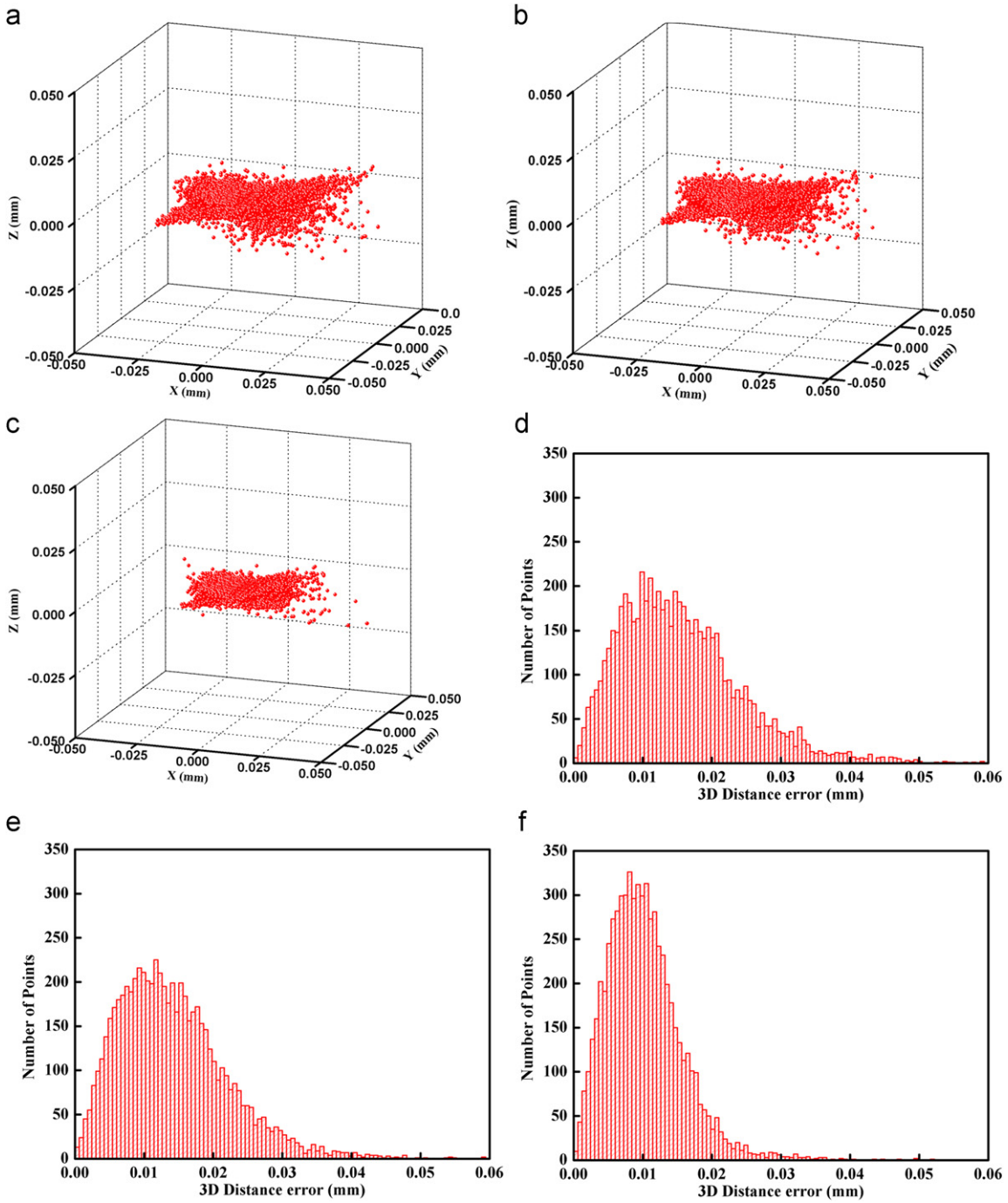

Fig. 16. 3D calibration error distribution and distance error statistics for testing data at different states: original, threshold selection and RANSAC. (a)–(c): the 3D error distribution for all the points; (d)–(f): the 3D distance error statistics for all the points. The computation of 3D calibration error can be referred to Eq. (7).

artificial illumination environment, respectively. The representative images are shown in Fig. 9. Note that the testing data is a set of nearly perfect images to evaluate the camera parameters obtained under natural or even worse conditions.

Fig. 10 shows the main procedure for outlier detection. We can observe that most of the feature points contaminated from illumination have been correctly identified after threshold selection and RANSAC carried out sequentially. In order to display the details of the detection result, we provide an enlarged part of the particular area denoted with a red line in Fig. 11. Clearly, the result indicates that the corners with uneven intensity level distribution are successfully determined. This outcome is quite similar to the simulative experiment discussed previously.

Table 2. shows the results of camera parameters and calibration accuracy obtained at different states. As Table 2 illustrated, calibration errors are significantly reduced after both the threshold selection and RANSAC strategies performed. Figs. 12 and 13 show the 2D and 3D calibration error distribution and statistics at different states for training data. As expected, the gross error distribution and distance error statistics gradually turn to produce a satisfactory outcome. In other words, more and more feature points manifest a small deviation to the corresponding computed ones and this phenomenon indicates a more accurate estimation for camera parameters.

In order to give the user a criterion when to choose the robust estimation method, we will discuss the consuming time of each step. In this study, we have carried out the real experiment on the following PC condition: Intel Core2 Quad CPU 2.40 GHz, Memory 2 GB, and the programming environment is Visual Studio 2010. The threshold selection step consumes time of 20.71 s and the RANSAC process consumes time of 13.45 s. It should be indicated that most of the time is consumed in the Levenberg–Marquardt non-linear optimization process and the time consumed by non-linear optimization is proportional to the number of feature points we want to optimize (the number of all the feature points in each image is 1296 in this paper). For example, to identify all the inliers during the RANSAC process only consumes 1.45 s and the remaining 13.00 s is consumed by non-linear optimization. In addition, since most camera calibration process is carried out off-line, we consider the computation time is not a major factor to take into account and the accuracy of the calibration is more important than it, especially for vision measurement.

To further investigate the validity of the proposed method, five testing images captured under ideal circumstance are employed to assess the precision of camera parameters. Since the testing images are not involved in the process of calibration, the evaluation results computed from testing data would be more persuasive than training data. Table 3 shows the results of calibration accuracy evaluated by testing data at different states. The comparative results of average calibration accuracy are also displayed as three bar charts with error bars shown in Fig. 14. Figs. 15 and 16 show the 2D and 3D calibration error distribution and distance error statistics at different states for testing data. From Table 3 and Figs. 14–16, we can recognize that the calibration accuracy is improved step by step compared with the original state. Statistically speaking, all the feature points' calculated coordinates are approaching the real ones after outlier removal, no matter which evaluation criterion is adopted. In addition, we can also find that the performance improvement brought by threshold selection step is relatively limited compared with the second RANSAC step. This is because the RANSAC method is able to exclude more outliers in a delicate way and promote the parameters to a more precise level. In short, the consequences mentioned above are consistent with simulative results or theoretical analysis and the merits of the proposed estimation method for camera parameters have been validated.

6. Conclusion

In this paper, an accurate and robust RANSAC-based estimation method for camera parameters is proposed. Up to now, the calibration technique based on multiple views of 2D planar target takes advantage of all the feature points even some of them have deviations. In that case, the camera parameters cannot represent the ideal pin-hole model and lens distortion model in an accurate way. To address this issue, we present an effective method to detect and handle the inaccurate or even incorrect feature points. First, feature points with extremely large noise are removed easily using the simple threshold method. Second, the remaining outliers in the calibration images are detected comprehensively by using RANSAC. Additionally, the camera parameters are adjusted to only inliers after each removal through non-linear optimization algorithm. With the proposed method, most of the outliers have been successfully excluded and the calibration errors are reduced. In order to validate the proposed method, four different evaluation functions are employed to test the performance of the estimated parameters. Results from the computer simulation and real experiment demonstrate the effectiveness of this method. It is especially suitable for camera calibration under the circumstances of uncontrollable environment or non-custom calibration board.

Acknowledgements

This work was supported by the National Natural Science Foundation of China (No. 61072134), the Research Fund for the Doctoral Program of Higher Education of China (No. 20101102110033) and the Pilot Foundation of Beihang University(No. YWF-11-02-261).

References

[1] Zhang Z, Matsushita Y, Ma Y. Camera calibration with lens distortion from low-rank textures. In: Proceedings of the IEEE Conference on Computer Vision and Pattern Recognition; 2011, p. 2321–2328.
[2] Tsai RY. A versatile camera calibration technique for high-accuracy 3D machine vision metrology using off the-shelf TV cameras and lenses. IEEE J Rob Autom 1987;RA-3:323–44.
[3] Miyagawa I, Arai H, Koike H. Simple camera calibration from a single image using five points on two orthogonal 1-D objects. IEEE Trans Image Process 2010;19:1528–38.
[4] Heikkila J. Geometric camera calibration using circular control points. IEEE Trans Pattern Anal Mach Intell 2000;22:1066–77.
[5] Zhang ZY. A flexible new technique for camera calibration. IEEE Trans Pattern Anal Mach Intell 2000;22:1330–4.
[6] Sun W, Cooperstock JR. An empirical evaluation of factors influencing camera calibration accuracy using three publicly available techniques. Mach Vision Appl 2006;17:51–67.
[7] Su J. Camera calibration based on receptive fields. Pattern Recognit 2007;40:2837–45.
[8] Weng J, Cohen P, Herniou M. Camera calibration with distortion models and accuracy evaluation. IEEE Trans Pattern Anal Mach Intell 1992;14:965–80.
[9] Xiao ZZ, Liang J, Yu DH, Tang ZZ, Asundi A. An accurate stereo vision system using cross-shaped target self-calibration method based on photogrammetry. Opt Lasers Eng 2010;48:1252–61.
[10] Zhou FQ, Zhang GJ. Complete calibration of a structured light stripe vision sensor through planar target of unknown orientations. Image Vision Comput 2005;23:59–67.
[11] Heikkila J, Silven O. A four-step camera calibration procedure with implicit image correction. In: Proceedings of the IEEE Conference on Computer Vision and Pattern Recognition; 1997, p. 1106–1112.
[12] Wu YH, Li YF, Hu ZY. Detecting and handling unreliable points for camera parameter estimation. Int J Comput Vision 2008;79:209–23.
[13] Douxchamps D, Chihara K. High-accuracy and robust localization of large control markers for geometric camera calibration. IEEE Trans Pattern Anal Mach Intell 2009;31:376–83.
[14] Schmalz C, Forster F, Angelopoulou E. Camera calibration: active versus passive targets. Opt Eng 2011;50:113601.
[15] Mallon J, Whelan PF. Which pattern? Biasing aspects of planar calibration patterns and detection methods. Pattern Recognit Lett 2007;28:921–30.

[16] Kruger L, Wohler C. Accurate chequerboard corner localisation for camera calibration. Pattern Recognit Lett 2011;32:1428–35.
[17] Yu CS, Peng QJ. Robust recognition of checkerboard pattern for camera calibration. Opt Eng 2006;45:093201.
[18] Ricolfe-Viala C, Sanchez-Salmeron AJ. Robust metric calibration of non-linear camera lens distortion. Pattern Recognit 2010;43:1688–99.
[19] Ricolfe-Viala C, Sanchez-Salmeron AJ. Lens distortion models evaluation. Appl Opt 2010;49:5914–28.
[20] Ricolfe-Viala C, Sanchez-Salmeron AJ, Martinez-Berti E. Accurate calibration with highly distorted images. Appl Opt 2012;51:89–101.
[21] Ji Q, Zhang YM. Camera calibration with genetic algorithms. IEEE Trans Syst Man Cybern Part A Syst Humans 2001;31:120–30.
[22] Ahmed MT, Hemayed EE, Farag AA. Neurocalibration: a neural network that can tell camera calibration parameters. In: Proceedings of the 7th IEEE International Conference on Computer Vision; 1999, p. 463–468.
[23] Stringa E, Regazzoni CS. A novel camera calibration algorithm based on Kalman filter. In: Proceedings of the 15th International Conference on Pattern Recognition; 2000, p. 872–875.
[24] Rahman T, Krouglicof N. An efficient camera calibration technique offering robustness and accuracy over a wide range of lens distortion. IEEE Trans Image Process 2012;21:626–37.
[25] Zhou F, Cui Y, Peng B, Wang Y. A novel optimization method of camera parameters used for vision measurement. Opt Laser Technol 2012;44: 1840–9.
[26] Ricolfe-Viala C, Sanchez-Salmeron A-J. Camera calibration under optimal conditions. Opt Express 2011;19:10769–75.
[27] Sutherland IE. Sketchpad: a man-machine graphical communications system. Technical Report 296. MIT Lincoln Laboratory; 1963.
[28] YI Abdel-Aziz, Karara, HM. Direct linear transformation from comparator coordinates into object space coordinates in close-range photogrammetry. In: Proceedings of the ASP/UI symposium on close range photogrammetry; 1971, p. 1–18.
[29] Hartley R, Zisserman A. Multiple View Geometry in Computer Vision. 2nd ed.Cambridge University Press; 2003.
[30] Fischler MA, Bolles RC. Random sample consensus: a paradigm for model fitting with applications to image analysis and automated cartography. Commun ACM 1981;24:381–95.
[31] Serradell E, Oezuysal M, Lepetit V, Fua P, Moreno-Noguer F. Combining geometric and appearance priors for robust homography estimation. In: Proceedings of the 11th European Conference on Computer Vision; 2010, p. 58–72.
[32] Zhai M, Fu S, Jing Z. Homography estimation from planar contours in image sequence. Opt Eng 2010;49:037202.
[33] Cheng C-M, Lai S-H. A consensus sampling technique for fast and robust model fitting. Pattern Recognit 2009;42:1318–29.
[34] Torr PHS, Murray DW. The development and comparison of robust methods for estimating the fundamental matrix. Int J Comput Vision 1997;24: 271–300.
[35] Torr PHS, Davidson C. IMPSAC: synthesis of importance sampling and random sample consensus. IEEE Trans Pattern Anal Mach Intell 2003;25: 354–64.
[36] Wan X, Xu G. Camera parameters estimation and evaluation in active vision system. Pattern Recognit 1996;29:439–47.
[37] Scaramuzza D. 1-point-RANSAC structure from motion for vehicle-mounted cameras by exploiting non-holonomic constraints. Int J Comput Vision 2011;95:74–85.
[38] Nister D. Preemptive RANSAC for live structure and motion estimation. Mach Vision Appl 2005;16:321–9.
[39] Naroditsky O, Zhou XS, Gallier J, Roumeliotis SI, Daniilidis K. Two efficient solutions for visual odometry using directional correspondence. IEEE Trans Pattern Anal Mach Intell 2012;34:818–24.
[40] Chen C-S, Hung Y-P, Cheng J-B. RANSAC-based DARCES: a new approach to fast automatic registration of partially overlapping range images. IEEE Trans Pattern Anal Mach Intell 1999;21:1229–34.
[41] González-Aguilera D, Rodríguez-Gonzálvez P, Hernández-López D, Luis Lerma J. A robust and hierarchical approach for the automatic co-registration of intensity and visible images. Opt Laser Technol 2012;44: 1915–23.
[42] Li Y, Gu L, Kanade T. Robustly aligning a shape model and its application to car alignment of unknown pose. IEEE Trans Pattern Anal Mach Intell 2011;33:1860–76.
[43] Lavva I, Hameiri E, Shimshoni I. Robust methods for geometric primitive recovery and estimation from range images. IEEE Trans Syst Man Cybern Part B Cybern 2008;38:826–45.
[44] Kim J-H, Han JH. Outlier correction from uncalibrated image sequence using the Triangulation method. Pattern Recognit 2006;39:394–404.
[45] Mai F, Hung YS, Zhong H, Sze WF. A hierarchical approach for fast and robust ellipse extraction. Pattern Recognit 2008;41:2512–24.
[46] Gallo O, Manduchi R, Rafii A. CC-RANSAC: Fitting planes in the presence of multiple surfaces in range data. Pattern Recognit Lett 2011;32:403–10.
[47] Raguram R, Frahm J-M, Pollefeys M. A comparative analysis of RANSAC techniques leading to adaptive real-time random sample consensus. In: Proceedings of the 10th European Conference on Computer Vision; 2008, p. 500–513.
[48] Chum O, Matas J. Optimal randomized RANSAC. IEEE Trans Pattern Anal Mach Intell 2008;30:1472–82.
[49] Matas J, Chum O. Randomized RANSAC with Td,d test. Image Vision Comput 2004;22:837–42.
[50] Frahm J-M, Pollefeys M. RANSAC for (Quasi-)Degenerate data (QDEGSAC). In: Proceedings of the IEEE Conference on Computer Vision and Pattern Recognition; 2006, p. 453–460.
[51] Scherer-Negenborn N, Schaefer R. Model fitting with sufficient random sample coverage. Int J Comput Vision 2010;89:120–8.
[52] Zhang Z, Zhu D, Zhang J, Peng Z. Improved robust and accurate camera calibration method used for machine vision application. Opt Eng 2008;47: 117201.
[53] Quan L, Lan Z. Linear N-point camera pose determination. IEEE Trans Pattern Anal Mach Intell 1999;21:774–80.
[54] Salvi J, Armangué X, Batlle J. A comparative review of camera calibrating methods with accuracy evaluation. Pattern Recognit 2002;35:1617–35.
[55] Triggs B. Autocalibration from planar scenes. In: Proceedings of the 5th European Conference on Computer Vision; 1998, p. 89–105.